

# Application of CAE, NSGA II Algorithm, And Multi-Criteria Decision-Making Methods in the Optimization of Hot Forging for SUS304 Valve Blanks

Pham Ngoc Linh<sup>1\*</sup>, Nguyen Van Quyen<sup>2\*</sup>

<sup>1</sup>Faculty of Mechanical Engineering, Hanoi University of Industry, Vietnam, 0100000

<sup>2</sup>Student, Faculty of Mechanical Engineering, Hanoi University of Industry, Vietnam, 0100000

Corresponding Author: quyenct2k1@gmail.com

**Abstract**— The study aims to enhance the efficiency of using CAE simulation technology in analyzing hot forging for SUS304 valve blanks. The simulation process utilizes three different input variables, forming a set of 15 simulations with two distinct output objectives. The results obtained from the CAE simulations will be used to construct a set of optimal solutions through the NSGA II algorithm. Subsequently, the TOPSIS method is applied to select the most optimal solution from the Pareto set of solutions. The chosen simulation software is QForm, which provides several desired results, including temperature, forging force, stress, durability, and defect analysis.

**Keywords**— QForm, Hot forging, FE Simulation, Stainless Steel Forging, Valve Forging, SVR, NSGA II, TOPSIS.

## I. INTRODUCTION

"According to the Ministry of Industry and Trade (2023), statistics reveal that the value of Vietnam's mold industry has exceeded USD 1 billion per year," indicating the immense potential for strong development in this field in the future. With an annual growth rate of 18%, the mold market in Vietnam has garnered significant attention from both domestic and international enterprises [1]. Hot forging molds play an essential role in the industry, particularly for components requiring high quality and durability, such as valves.

Today, CAE analytical tools are advancing rapidly, and various optimization methods are available. The combination of these methods contributes to enhancing efficiency, improving product quality, shortening production time, and minimizing errors in the manufacturing process. According to reports, the production process of SUS304 valve blanks [2], is well-suited to closed-die forging. Closed-die forging is applied to various materials, such as AISI4150 automotive steering joints [3], 20CrMnTi planetary differential gears [4], AISI4130 bevel gears [5], aluminum alloy rotors [6], Nimonic 80 large exhaust valves [7], motorcycle engines [8], and gears. Its outstanding advantages include reduced scrap and superior durability. Simulation software is often the most accurate choice for optimizing forging dies and designing blanks to reduce design time and improve economic efficiency [9].

The research was conducted using QForm UK 11.0.1 simulation software, which applies various theories to the simulation process, notably the finite element method (Figure 1.1) and plastic deformation (Figure 1.2) [10]. The goal is to determine the optimal die based on predicted results for the required forging force and tool durability. Subsequently, SVR, the NSGA II algorithm, and the TOPSIS method are applied to propose an optimal solution.

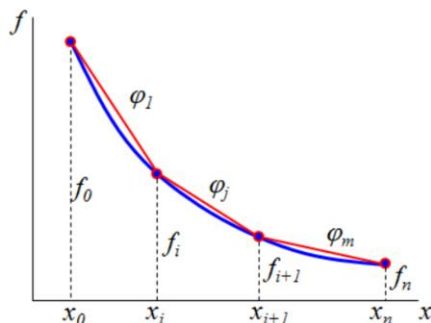


Figure 1.1. Diagram depicting finite element method

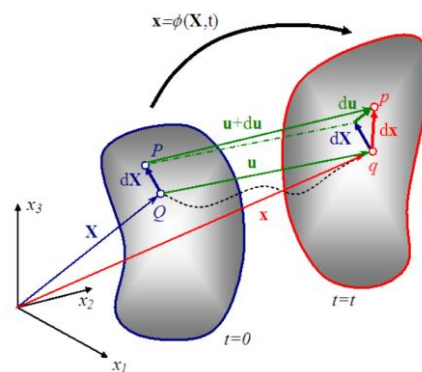


Figure 1.2 Description of geometric plastic deformation.

The finite element method applies (Equation (1.1)) [10].

$$f(x) = \sum_{m=1}^M \varphi_m(x); \varphi_m(x) = \frac{f_{n+1} - f_n}{x_{n+1} - x_n} (x - x_n) \quad (1.1)$$

In addition, there are several other related scientific theories such as friction in the process of plastic deformation (Figure 1.3) [10].

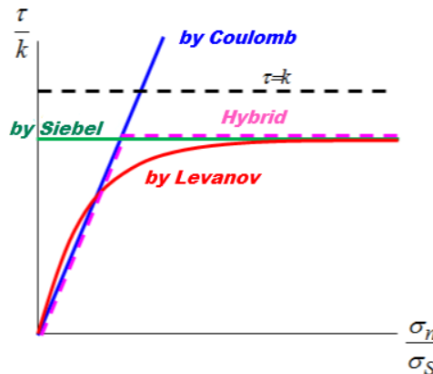


Figure 1.3. Charts the crossover between friction theories.

## II. APPLICATION OF CAE

### a. Materials of workpieces and dies

The chemical composition percentages of the billet material are SUS304 (Table 2.1) and the die material is SKD11 (Table 2.2).

Table 2.1. The chemical composition of JIS stainless steel SUS 304 in percent

C	Yes	Mn	P	S	N	Cr	Ni
< 0.07	< 1	< 2	< 0.045	< 0.015	< 0.11	17.5÷19.5	8÷10.5

Table 2.2. The chemical composition of SKD11 in percent

C	Si	Mn	P	S	Cr	Mo	V
0.35÷0.45	0.9÷1.2	0.25÷0.55	< 0.03	< 0.03	4.5÷5.5	1.2÷1.7	0.85÷1.15

### b. Input parameters

The fixed parameters during the experiment are presented in (Table 2.3).

Table 2.3. Forging process parameters

	Raw-Forging
Workpiece material	SUS304
The material	H13
Load	6.3 MN
Lubrication	Graphite + water

The changing parameters (input variables) include billet temperature, die temperature, and the stopping distance of Tool 2 (central punch) during the forming process of the billet with Tool 3 (side punch).

- +  $X_1$ : Initial billet temperature (°C)
- +  $X_2$ : Initial die temperature (°C)
- +  $X_3$ : Stopping distance of Tool 2 (mm)

The objective functions are determined as the forging force of Tool 2 and the wear cycle 5% of Tool 2, denoted as  $Y_1$  and  $Y_2$  respectively. After identifying the variables, the parameter values for the objective functions are established (Table 2.4).

Table 2.4. Simulation Data

STT	$X_1$ (°C)	$X_2$ (°C)	$X_3$ (mm)
1	1000	200	34
2	1000	180	32
3	1000	220	32
4	1000	200	30
5	1100	200	32
6	1100	200	32
7	1100	180	30
8	1100	220	34
9	1100	220	30
10	1100	200	32
11	1100	180	34

12	1200	180	32
13	1200	220	32
14	1200	200	30
15	1200	200	34

c. Simulation process in QForm

The four main steps of a simulation process in QForm 10 are shown in (Figure 2.1) [11].

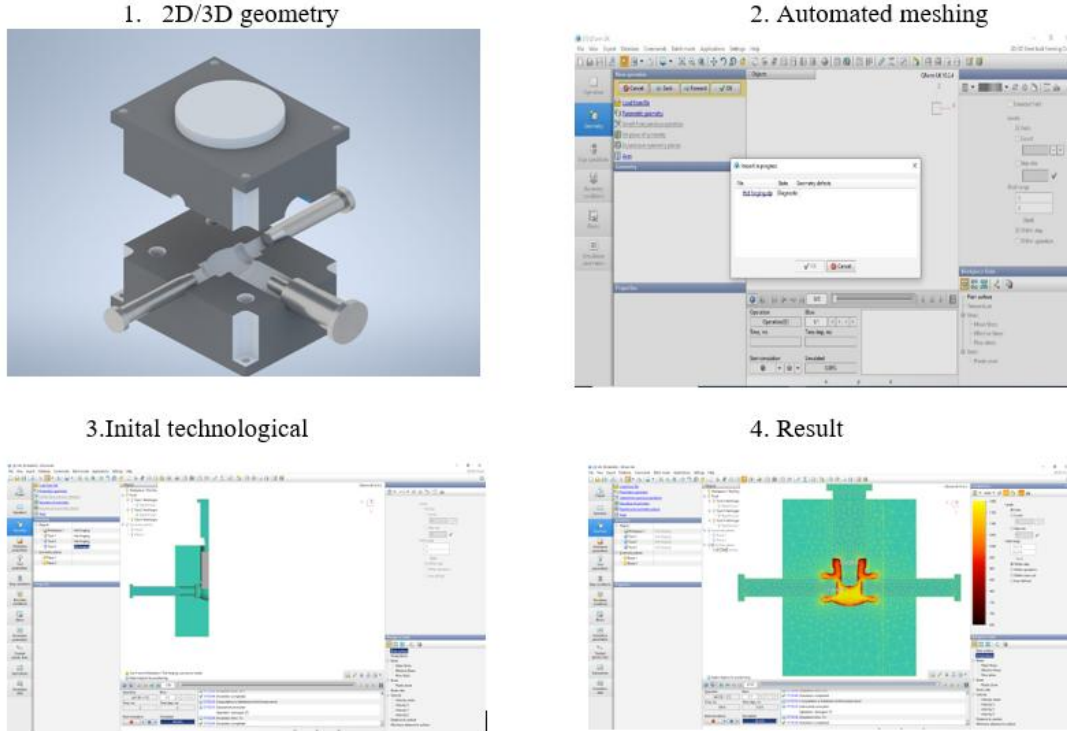
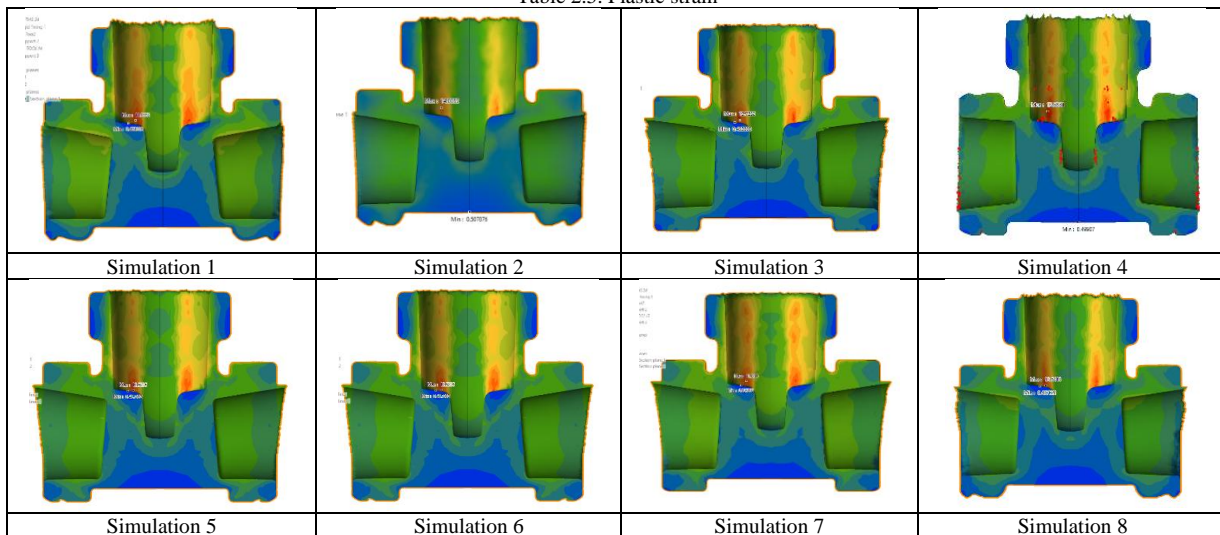


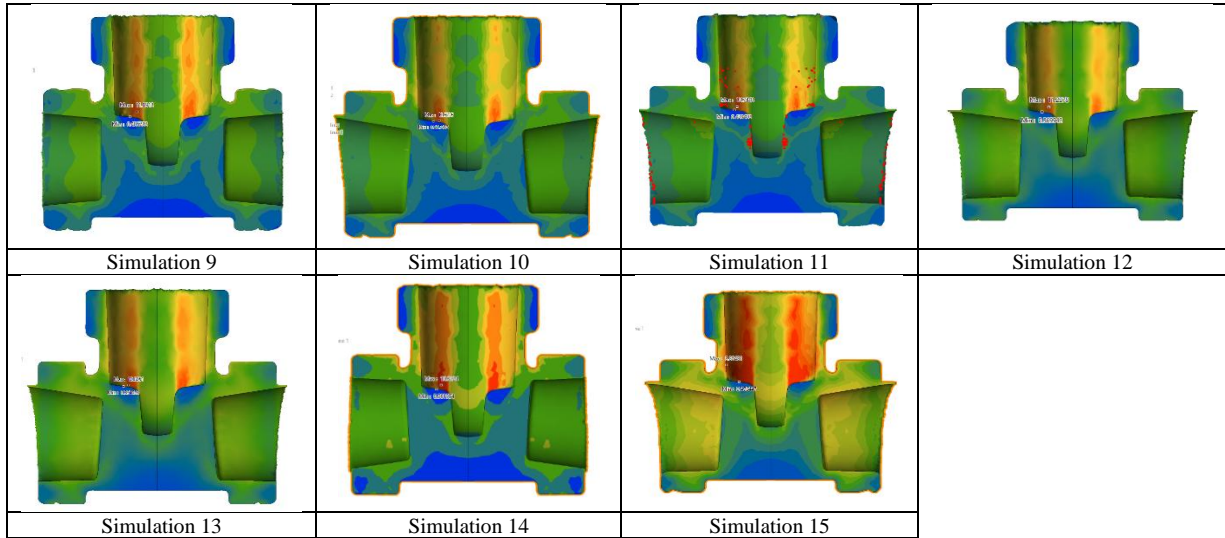
Figure 2.1. Simulation process in QForm software

d. Results and discussion

2.4.1 Plastic strain

Table 2.5. Plastic strain

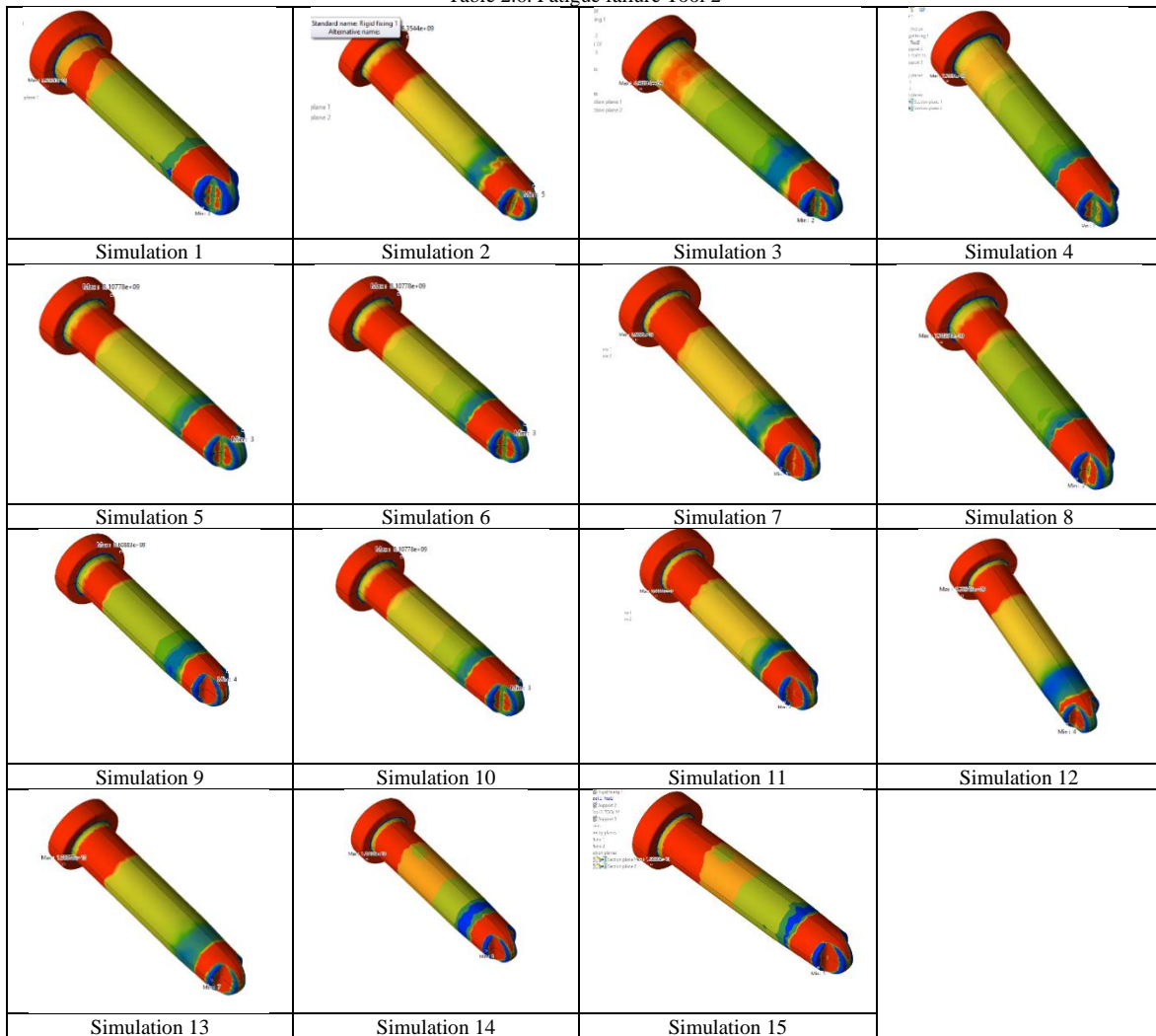




In (Table 2.5) the orange color indicates large deformation, while the blue color represents small deformation. The results show that the highest plastic deformation occurs on both sides of the neck of the part, where the material excessively recovers, causing the material flow to spread to both sides.

2.4.2 Fatigue failure Tool 2

Table 2.6. Fatigue failure Tool 2



From the results of 15 simulation experiments, the author selects one experiment for evaluation, and in simulation experiment 5, the variable values are set at the midpoint within their respective ranges. The die's durability is evaluated based on the percentage of die volume wear after the forging cycles.

With 5% volume wear occurring after 2 968 forging cycles, the factory needs to maintain the die to ensure that the product quality continues to meet the required standards (Figure 2.2).

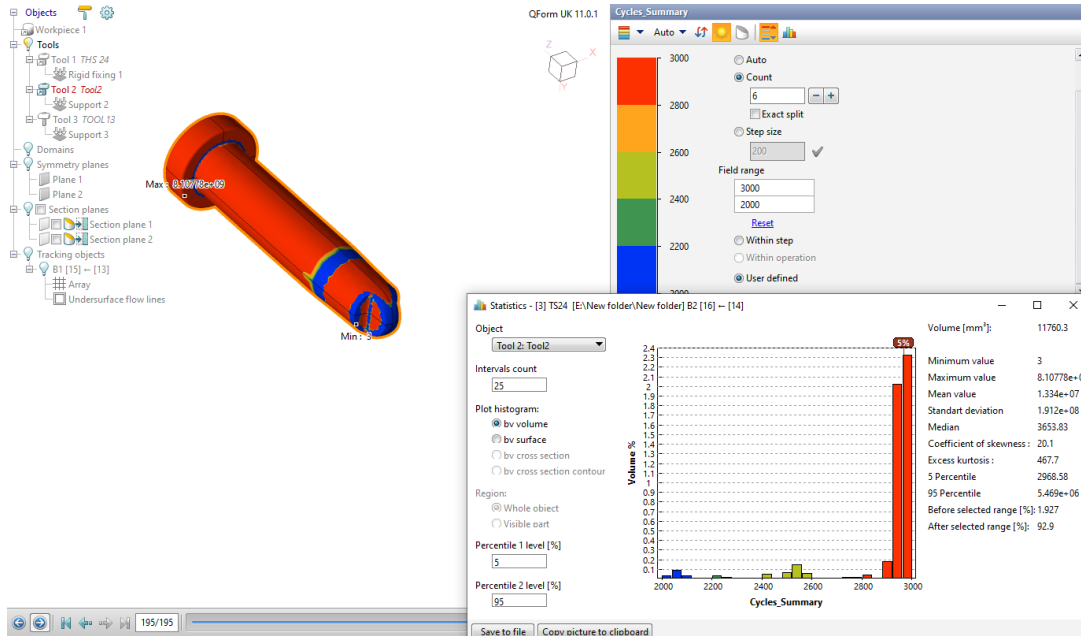
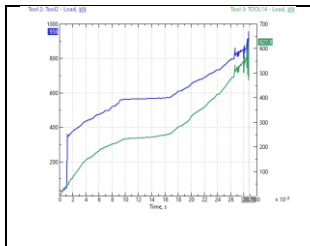
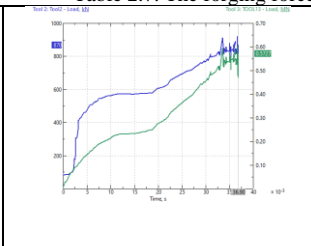
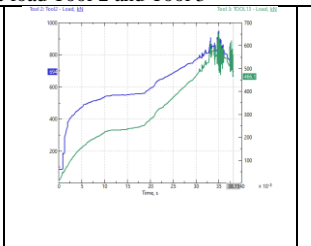
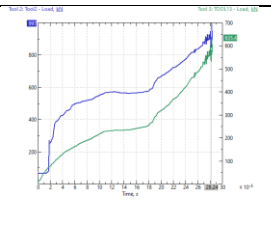
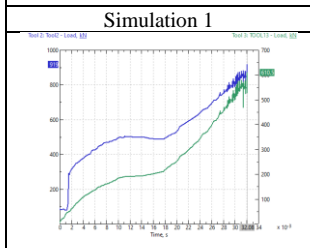
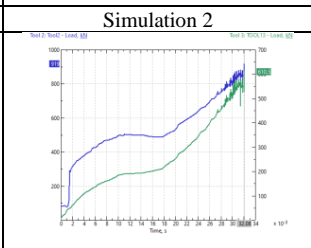
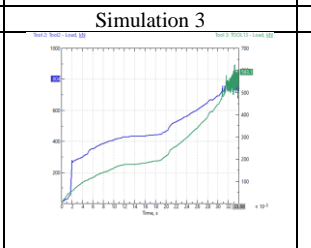
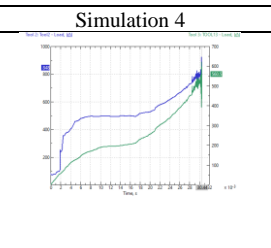
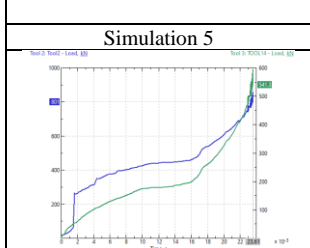
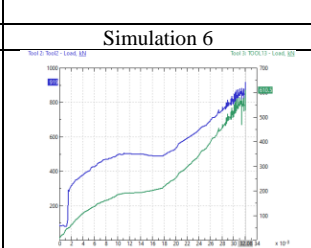
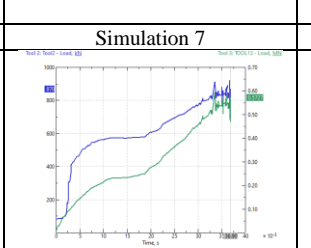
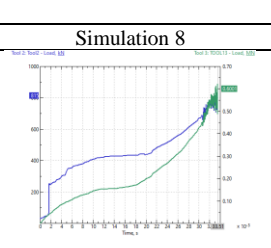
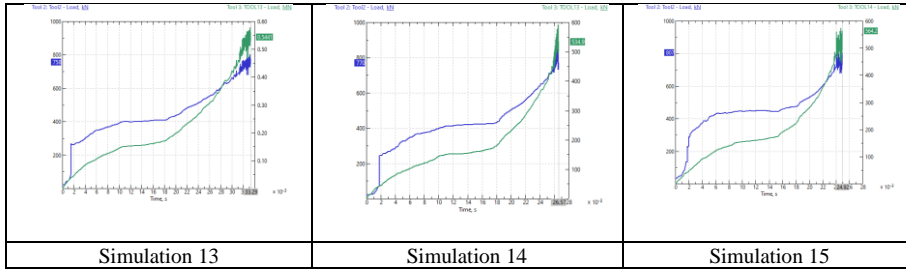


Figure 2.2. Wear diagram as a percentage of the volume of the Tool 2

### 2.4.3 The forging force load

Table 2.7. The forging force load Tool 2 and Tool 3

			
Simulation 1	Simulation 2	Simulation 3	Simulation 4
			
Simulation 5	Simulation 6	Simulation 7	Simulation 8
			
Simulation 9	Simulation 10	Simulation 11	Simulation 12



Tool 2: Tool2 - Load, kN

Tool 3: TOOL13 - Load, kN

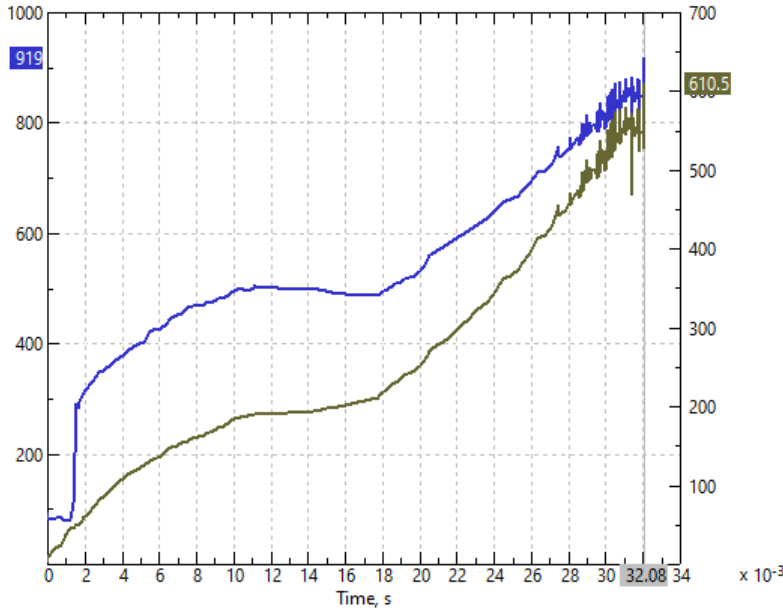


Figure 2.3. The relationship between forging force and the distance of Tool 2 and Tool 3

With the complex profile of the valve, the forging force of the punch fluctuates in the final stage to fully fill the die. The blue line represents the force of Tool 2, which shows a sharp increase at the beginning and stabilizes later, while the brown line represents the force of Tool 3, which increases steadily throughout.

### III. SVR-NSGA II-TOPSIS

#### a. Support Vector Regression

SVR stands for "Support Vector Regression," a machine learning algorithm applied to regression analysis. The model in SVR aims to find a function that approximates the relationship between input variables and a continuous target variable while minimizing prediction error [12].

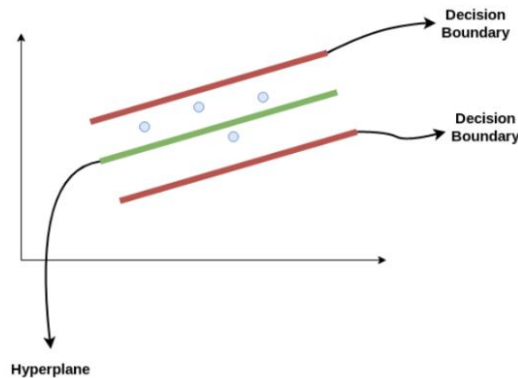


Figure 3.1.

Hình 3.1. SVR Regression Function Chart [12]

The hyperplane lies between two boundary lines with distances of 'a' and '-a'. The distance 'a' is referred to as epsilon. The regression function problem is based on the equations below [12].

The SVR regression function is represented by Equation (3.1):  

$$Y = Wx + b \tag{3.1}$$

The decision boundary equations are based by Equation (3.2) and (3.3):

$$Wx + b = a \tag{3.2}$$

$$Wx + b = -a \tag{3.3}$$

Any equation must satisfy the conditions by Equation (3.4):

$$-a < (Y - Wx + b) < +a \tag{3.4}$$

The loss function equation L (y f (x, w)) (3.5) is referred to as epsilon-loss:

$$L = \begin{cases} 0 & \text{if } |y - f(x, w)| \leq \varepsilon \\ |y - f(x, w)| & \text{otherwise} \end{cases} \tag{3.5}$$

This means that:

- + Errors smaller than  $\varepsilon$  will not be included in the loss function.
- + Errors greater than  $\varepsilon$  will be penalized.

The SRV problem is formulated as an optimization problem defined by Equation (3.6).

$$\min \frac{1}{2} \|w\|^2 + C \cdot \sum_{i=1}^n (\zeta_i + \zeta_i^*) \tag{3.6}$$

With the constraints defined by Equation (3.7):

$$\begin{cases} y_i - f(x_i, w) \leq \varepsilon + \zeta_i^* \\ f(x_i, w) - y_i \leq \varepsilon + \zeta_i \\ \zeta_i, \zeta_i^* > 0 \forall i = 1, \dots, n \end{cases} \tag{3.7}$$

Applying the duality theorem to minimize the problem, we ultimately derive the function f(x) in Equation (3.8):

$$f(x) = \sum_{i=1}^m (\alpha_i - \alpha_i^*) \cdot K(x_i, x) + b \tag{3.8}$$

Where nSV represents the number of support vectors, and the kernel function, denoted as K, is defined by Equation (3.9):

$$K(x_i, x) = \sum_{j=1}^m g_j(x_i) \cdot g_j(x) \tag{3.9}$$

### 3.1.1 Defining the problem

The specific optimization problem is as follows: Find  $X = [X_1, X_2, X_3]$  to minimize  $\{Y_1\}$  and maximize  $\{Y_2\}$  subject to the constraints in Equation (3.10):

$$\begin{cases} 1000 \leq X_1 \leq 1200 \\ 180 \leq X_2 \leq 220 \\ 30 \leq X_3 \leq 34 \end{cases}$$

Using SRV to establish a regression model linking  $Y_1, Y_2$  with the parameters  $X_1, X_2, X_3$ . This model will serve as the foundation for multi-objective optimization using NSGA II.

The data collected from the QForm simulation results is presented in (Table 3.1):

Table 3.1. Simulation Results

STT	$X_1$ (°C)	$X_2$ (°C)	$X_3$ (mm)	$Y_1$ (kN)	$Y_2$ (chu ký)
1	1000	200	34	956	2857
2	1000	180	32	870	3075
3	1000	220	32	694	2485
4	1000	200	30	997	2536
5	1100	200	32	919	2968
6	1100	200	32	919	2968
7	1100	180	30	804	3175
8	1100	220	34	848	2757
9	1100	220	30	801	2763
10	1100	200	32	919	2968
11	1100	180	34	764	3400
12	1200	180	32	815	2446
13	1200	220	32	758	2778
14	1200	200	30	770	3006
15	1200	200	34	807	3195

After applying SVR to establish the regression model for the problem and inputting the data into the software as detailed in Appendix 1, the results are presented in (Table 3.2).

From the results table, the regression chart with two objective functions is obtained, as shown in Figure 3.2.

Table 3.2. SRV Results

STT	$X_1$ (°C)	$X_2$ (°C)	$X_3$ (mm)	$Y_1$ -simulated (kN)	$Y_2$ -simulated (chu kỳ)	$Y_1$ -Predict (kN)	$Y_2$ -Predict (sản phẩm)
1	1000	200	34	956	2857	896.470	2883
2	1000	180	32	870	3075	861.803	3049
3	1000	220	32	694	2485	808.958	2556
4	1000	200	30	997	2536	896.639	2684
5	1100	200	32	919	2968	910.782	2942
6	1100	200	32	919	2968	910.782	2942
7	1100	180	30	804	3175	812.222	3105
8	1100	220	34	848	2757	839.764	2783
9	1100	220	30	801	2763	809.188	2769
10	1100	200	32	919	2968	910.782	2942
11	1100	180	34	764	3400	791.514	3199
12	1200	180	32	815	2446	806.803	2894
13	1200	220	32	758	2778	766.193	2804
14	1200	200	30	770	3006	778.245	2980
15	1200	200	34	807	3195	814.738	3113

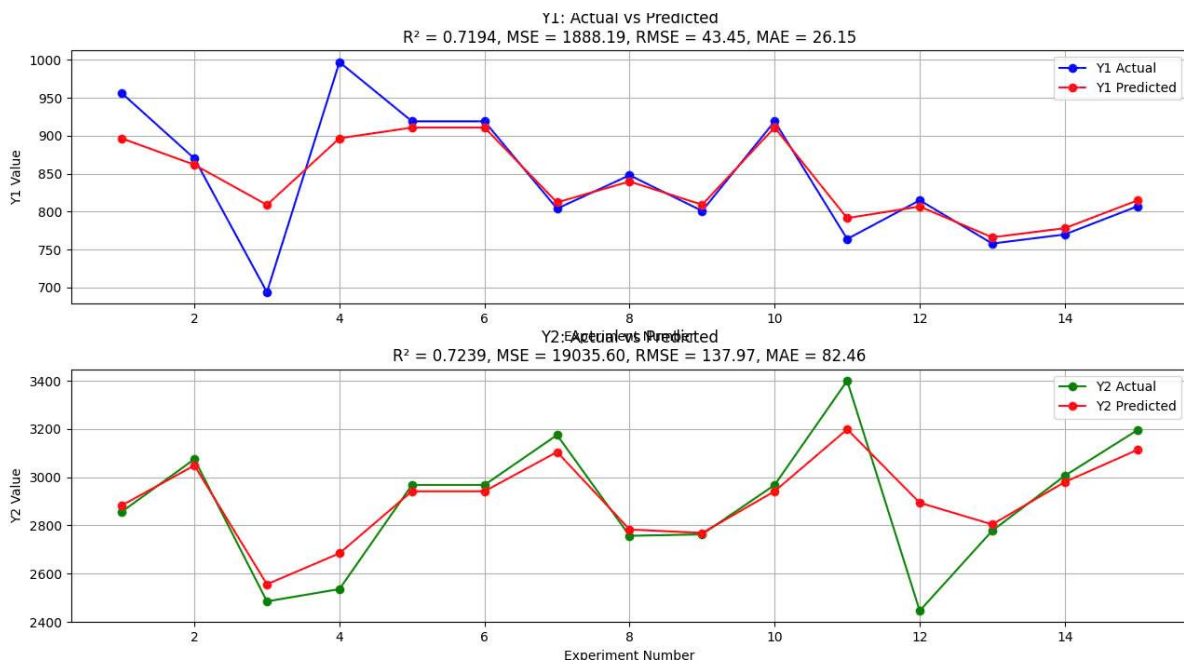


Figure 3.2. Chart of the objective functions: Forging Force and 5% Volume Wear Cycle of Tool 2 (product).

From the figure, it shows that the simulated data is close to the predicted data.

Analysis of the forging force chart shows two curves:

- +  $Y_1$ - Simulated (blue): Data from simulations.
- +  $Y_1$ -Predict (red): Predicted data.

Analysis of the 5% volume wear cycle chart for Tool 2 shows two curves:

- +  $Y_2$ - Simulated (green): Data from simulations.
- +  $Y_2$ -Predict (red): Predicted data.

The correlation between the two curves is very close across all simulations. The red curve demonstrates higher prediction accuracy for both the forging force and the 5% volume wear cycle compared to the actual simulation data.

b. NSGA II

From the SVR data combined with the NSGA-II algorithm, the multi-objective optimization results peak in a Pareto set, as shown in Figure 3.3.



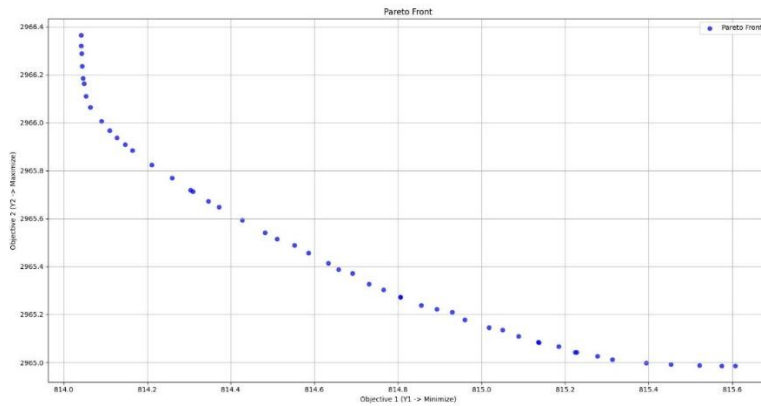


Figure 3.3. Pareto Chart

The horizontal axis represents the forging force  $Y_1$  while the vertical axis represents the 5% volume wear cycle  $Y_2$ . The set of optimal points forms a concave Pareto curve, where a decrease in forging force ( $Y_1$ ) corresponds to a gradual decrease in the wear cycle of Tool 2 ( $Y_2$ ). This indicates a trade-off relationship between  $Y_1$  and  $Y_2$ . If the goal is to increase the lifespan  $Y_2$  the forging force  $Y_1$  must decrease. Conversely, if the forging force  $Y_1$  is to be increased, the 5% wear cycle will decrease.

c. TOPSIS

Evaluating the Pareto set using TOPSIS requires entropy weights to determine the optimal values.

The steps for the TOPSIS method [13] are as follows.

Step 1: Construct the Decision Matrix with the Determined Elements.

$$X = \begin{bmatrix} x_{11} & \dots & x_{1j} & x_{1n} \\ x_{21} & \dots & x_{2j} & x_{2n} \\ \dots & \dots & \dots & \dots \\ x_{i1} & \dots & x_{ij} & x_{in} \\ \dots & \dots & \dots & \dots \\ x_{m1} & \dots & x_{mj} & x_{mn} \end{bmatrix} \quad (3.10)$$

Where:

- +  $x_{ij}$ : The value of the j criterion for the i alternative.
- + n: Number of criteria.
- + m: Number of alternatives.

Step 2: Normalize the Decision Matrix, where  $p_{ij}$  is determined as follows:

$$p_{ij} = \frac{x_{ij}}{\sqrt{\sum_{i=1}^m x_{ij}^2}}, j \in [1, n] \quad (3.11)$$

Step 3: The entropy  $e_i$  of the i criterion is determined as follows:

$$e_i = -\frac{1}{\ln(m)} \sum_{i=1}^m p_{ij} \ln(p_{ij}), i = 1 \dots m; j = 1 \dots n \quad (3.12)$$

Where:

- + entropy  $e_i$  lies within the range [0, 1].

A higher  $e_i$  indicates greater differentiation for the I criterion, meaning more information can be gathered from that criterion. Therefore, a higher weight should be assigned to that criterion. Subsequently, the weight  $w_i$  for the i criterion is calculated using the following Equation 3.13:

$$w_i = \frac{1-e_i}{\sum_{i=1}^m (1-e_i)} \quad (3.13)$$

Step 4: Calculate and construct the weighted normalized decision matrix, which is computed using the following Equation 3.14

$$Y = w_j \cdot p_{ij} \quad (3.14)$$

Where:

- +  $w_j$  is the weight of criterion j

Step 5: Identify the Best and Worst solutions

$$A^+ = \{y_1^+, y_2^+, \dots, y_j^+, \dots, y_n^+\} \quad (3.15)$$

$$A^- = \{y_1^-, y_2^-, \dots, y_j^-, \dots, y_n^-\} \quad (3.16)$$

Where:

- +  $y_j^+$  The best alternative for criterion j

+  $y_i^-$  The worst alternative for criterion j

Step 6: Calculate the positive ideal value  $S_i^+$  and the negative ideal value  $S_i^-$  the following Equations:

$$S_i^+ = \sqrt{\sum_{j=1}^n (y_{ij} - y_j^+)^2} \quad i = 1, 2, \dots, m \quad (3.17)$$

$$S_i^- = \sqrt{\sum_{j=1}^n (y_{ij} - y_j^-)^2} \quad i = 1, 2, \dots, m \quad (3.18)$$

Step 7: Determine the criteria and evaluate  $C_i^*$

$$C_i^* = \frac{S_i^-}{S_i^+ + S_i^-} \quad i = 1, 2, \dots, m; \quad 0 \leq C_i^* \leq 1 \quad (3.19)$$

Step 8: Rank  $C_i^*$  to select the best alternative.

The summary table of the optimization results using the combined SVR-NSGA II-TOPSIS algorithm is presented in (Table 3.3).

Table 3.3 SVR-NSGA II-TOPSIS results

STT	$X_1$ (°C)	$X_2$ (°C)	$X_3$ (mm)	$Y_1$ –Predict (kN)	$Y_2$ -Predict (chu kỲ)
4	1098.27	181.90	33.93	801.449	3202
6	1107.76	181.05	33.90	795.422	3199
13	1128.83	182.31	33.92	794.125	3188
22	1123.52	180.29	33.91	788.395	3185
17	1129.06	180.23	33.92	786.951	3179
5	1149.96	180.71	33.98	785.611	3154
16	1152.23	180.45	34.00	784.694	3150
25	1191.69	196.17	30.01	784.176	2998
10	1197.48	194.23	30.01	782.486	2997
2	1197.89	200.26	30.16	781.094	2974
8	1195.66	201.56	30.07	779.939	2973
1	1188.04	206.04	30.05	779.771	2949
7	1188.53	206.34	30.06	779.316	2947
11	1197.80	206.53	30.23	775.653	2939
9	1198.35	210.38	30.09	770.839	2919
18	1199.81	211.74	30.32	769.296	2901
3	1197.18	213.79	30.04	768.790	2899
24	1196.70	214.18	30.17	768.323	2891
23	1199.90	213.60	30.48	767.435	2881
21	1198.81	217.92	30.01	766.934	2877
20	1196.41	217.93	30.24	765.824	2865
14	1196.79	216.74	30.42	765.589	2863
12	1199.97	218.99	30.24	764.470	2861
15	1199.29	218.20	30.86	762.568	2834
19	1199.08	219.82	31.52	762.544	2805

Applying the TOPSIS method, the prediction errors for  $Y_1$  and  $Y_2$  are calculated based on the differences between the predicted and simulated values. The results, including the values of  $S_i^+$ ,  $S_i^-$ ,  $C_i^*$  are presented in (Table 3.4).

Table 3.4. The values of  $S_i^+$ ,  $S_i^-$ ,  $C_i^*$ , Rank

STT	$Y_1$ –Predict (kN)	$Y_2$ -Predict (chu kỲ)	$S_i^+$	$S_i^-$	$C_i^*$	TOPSIS Rank
4	801.449	3202	0.00	1.41	1.00	1
6	795.422	3199	0.16	1.30	0.89	2
13	794.125	3188	0.19	1.26	0.87	3
22	788.395	3185	0.34	1.17	0.78	4
17	786.951	3179	0.38	1.13	0.75	5
5	785.611	3154	0.42	1.06	0.71	6
16	784.694	3150	0.45	1.04	0.70	7
25	784.176	2998	0.68	0.74	0.52	8
10	782.486	2997	0.71	0.70	0.50	9
2	781.094	2974	0.78	0.64	0.45	10
8	779.939	2973	0.80	0.62	0.43	11
1	779.771	2949	0.85	0.57	0.40	12
7	779.316	2947	0.86	0.56	0.39	13
11	775.653	2939	0.94	0.48	0.34	14
9	770.839	2919	1.06	0.36	0.25	15
18	769.296	2901	1.12	0.30	0.21	16
3	768.790	2899	1.13	0.29	0.20	17
24	768.323	2891	1.16	0.26	0.18	18
23	767.435	2881	1.19	0.23	0.16	19

21	766.934	2877	1.21	0.21	0.15	20
20	765.824	2865	1.25	0.17	0.12	21
14	765.589	2863	1.26	0.17	0.12	22
12	764.470	2861	1.28	0.15	0.10	23
15	762.568	2834	1.36	0.07	0.05	24
19	762.544	2805	1.41	0.00	0.00	25

The results confirm that value 4 in the set of 25 optimal Pareto values shows a very far distance from the non-ideal solution and a very close distance to the ideal solution. The distance to the ideal solution ranges from 0 to 1.41.

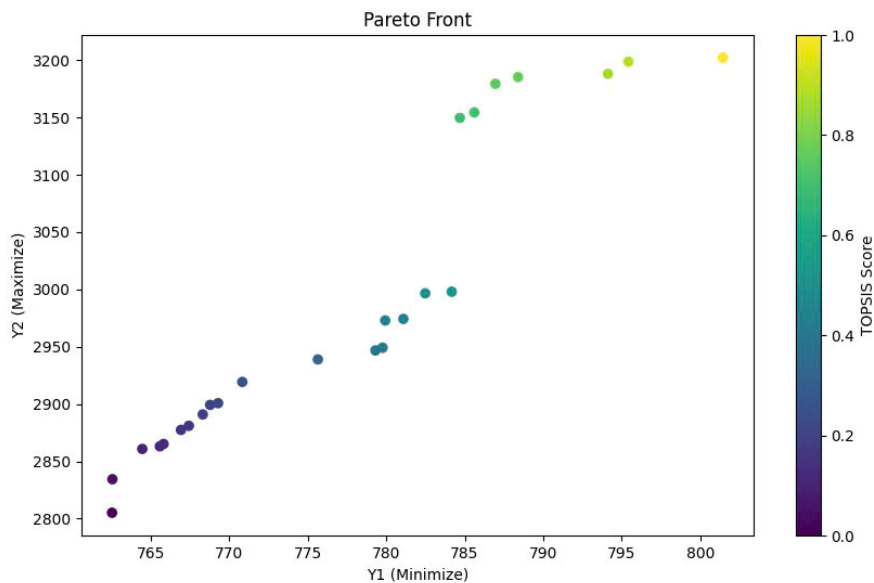


Figure 3.4. Pareto Front

From the results in Table 3.4 and Figure 3.4 the author selects the most optimal solution with the following values:

$$X_1 = 1098,27 \text{ (}^\circ\text{C)}$$

$$X_2 = 181,90 \text{ (}^\circ\text{C)}$$

$$X_3 = 33,93 \text{ (mm)}$$

#### IV. CONCLUSION

This is a significant research direction in the mold manufacturing industry, helping to evaluate product quality and save time, thereby enhancing competitiveness. CAE software provides substantial efficiency in analyzing product quality, die durability, and forging force, which assists in selecting appropriate production lines and determining the optimal maintenance schedule for equipment.

The NSGA II algorithm has been successfully applied to identify Pareto optimal solutions, while the multi-criteria decision-making method TOPSIS has thoroughly resolved the issue, enabling the selection of the best solution. In this study, the author successfully demonstrated the effectiveness of combining SVR with NSGA-II and TOPSIS in the multi-objective optimization process of hot forging for SUS304 valve blanks. The integration of SVR, NSGA-II, and entropy-weighted TOPSIS holds potential for applications beyond the hot forging process, providing a powerful tool for multi-objective optimization in computational research.

This research direction can be similarly applied to other components in the die, such as side punches, and to valves made from other materials like copper, aluminum alloys, and titanium. Furthermore, integrating advanced technologies, such as artificial intelligence (AI), can improve the performance of the NSGA II algorithm, bringing greater value in decision-making processes.

#### REFERENCES

- [1] <https://moit.gov.vn/tin-tuc/phat-trien-cong-nghiep/cong-nghiep-khuon-mau-tao-dong-luc-phat-trien-nganh-cong-nghiep-ho-tro.html>.
- [2] J. Yin, R. Hu, and X. Shu (2021), "Closed-die forging process of copper alloy valve body: Finite element simulation and experiments," *J. Mater. Res. Technol.*, vol. 10, pp. 1339–1347.
- [3] Q. Chen *et al.* (2019), "Isothermal closed-die forming process of magnesium alloy upper receiver: numerical simulation and experiments," *Int. J. Adv. Manuf. Technol.*, vol. 102, no. 1–4, pp. 685–694.
- [4] D. Y. Zhao, L. D. Zhang, H. X. Sun, and L. N. Sun (2010), "Research on precision forming technology of car steering knuckle,"
- [5] Y. Zhang, J. Huang, X. Lin, and Q. Fang (2008), "Numerical simulation analysis on cold closed-die forging of differential satellite gear in car,"

- [6] J. H. Song and Y. T. Im (2007), "Process design for closed-die forging of bevel gear by finite element analyses,".
- [7] L. Bai *et al.* (2022), "Experimental Study and Numerical Simulation of Polymer Flooding," *Fluid Dyn. Mater. Process.*, vol. 18, no. 6, pp. 1815–1826.
- [8] H. S. Jeong, J. R. Cho, and H. C. Park (2005), "Microstructure prediction of Nimonic 80A for large exhaust valve during hot closed die forging,"
- [9] X. Huang, Y. Zang, H. Ji, B. Wang, and H. Duan (2022), "Combination gear hot forging process and microstructure optimization,".
- [10] <https://qform3d.com/>
- [11] N. Van Canh, P. Van Kien, N. Trung, ... T. T.-I. J. of, and U. (2023), "Application of CAD/CAM/CAE in modelling of Die for Hot Forging of Stainless Steel Valve,"
- [12] Alakh, "Support Vector Regression Tutorial for Machine Learning,"
- [13] C. Hwang, Y. Lai, T. L.-C. & operations research, and undefined 1993, "A new approach for multiple objective decision making,".